POWER2019-1902

USING THERMODYNAMICS PRINCIPLES TO OPTIMIZE PERFORMANCE OF CAPACITIVE MIXING CYCLES FOR SALINITY GRADIENT ENERGY GENERATION

Daniel Moreno¹, Marta C. Hatzell¹

¹The G. W. Woodruff School of Mechanical Engineering Georgia Institute of Technology Atlanta, GA 30332 *Corresponding author: marta.hatzell@me.gatech.edu

ABSTRACT

Understanding the thermodynamics associated with ion mixing and separation processes is important in order to meet the rising demands for clean energy and water production. Several electrochemical-based technologies such as capacitive deionization and capacitive mixing (CapMix) are capable of achieving desalination and energy production through ion mixing and separation processes, yet experimental investigations suggest energy conversion occurs with low second law (thermodynamic) efficiency. Here, we explore the maximum attainable efficiency for different CapMix cycles to investigate the impact cycle operation has on energy extraction. All investigated cycles are analogous to well documented heat engine cycles. In order to analyze CapMix cycles, we develop a physics-based model of the electric double layer based on the Gouy-Chapman-Stern theory. Evaluating CapMix cycles for energy generation revealed that cycles where ion mixing occurs at constant concentration and switching occurs at constant charge (a cycle analogous to the Stirling engine) attained the highest overall first law (electrical energy) efficiency (39%). This first law efficiency is nearly 300% greater than the first law efficiency of the Otto, Diesel, Brayton, and Atkinson analog cycles where ion mixing occurs while maintaining a constant number of ions. Additionally, the maximum first law efficiency was 89% with a maximum work output of 0.5 kWh per m³ of solution mixed (V=1.0V) using this same Stirling cycle. Here the salinity gradient was C_H = 600 mM and C_L = 1 mM (ΔG_{mix} =0.56 kWh/m^3). The effect of voltage was also examined at $C_H = 600$ mM (seawater) and $C_L = 20$ mM (river water). CapMix cycles operated at lower voltage (V < 1.0V), resulted in the Otto cycle yielding the highest first law efficiency of approximately 25% (compared to under 20% for the Stirling cycle); however, this was at the expense of a reduction (50x) in net electrical energy extracted from the same mixing process (0.01 kWh per m³).

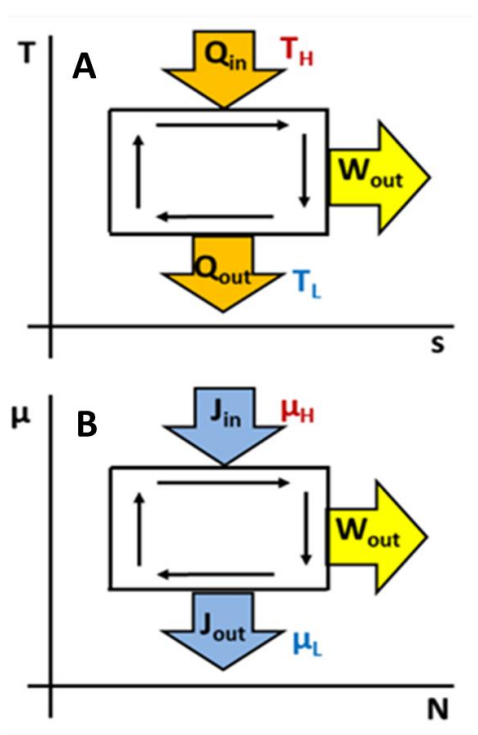


Figure 1. (a) Thermodynamic heat engine cycle, and (b) blue engine cycle.

INTRODUCTION

The increasing electrification of energy and water systems promotes investigating technologies, which convert energy directly into electricity [1]. This is in contrast with most modern energy systems (heat engines), where power production occurs through converting thermal energy into mechanical energy prior to electricity generation (Figure 1a) [2]. While effective, the numerous conversion processes promote excess loss. In addition, the maximum obtainable efficiency is limited by the temperature

of a thermal reservoir (Carnot limitation). Another welldocumented limitation with power generation systems is that they produce a significant amount of carbon emissions if fossil fuels are used to produce heat. This promotes the development of higher efficiency energy systems, which convert chemical energy directly to electricity.

Chemical to electrical energy conversion processes occur primarily using electrochemical-based technologies, and extract work based on the flow of ions (Figure 1b). Mixing energy extracted from this process is often termed "blue energy" [3]. Various approaches exist for extracting mixing energy, such as reverse electrodialysis and pressure retarded osmosis. However, capacitive-based technologies have emerged as a potential low cost approach for generating energy through ion mixing processes [4].

In CapMix, electrical energy is produced through storing and releasing ions within an electric double layer (EDL) at a high surface area charged electrode [5, 6]. Controlled ion mixing occurs through charging the electrodes in a high concentration stream (C_H), and discharging the electrodes in a second low concentration stream (C_L). In a low concentration stream, the diffuse portion of the EDL expands resulting in a reduction in electrode capacitance. This reduction in the electrode capacitance causes an increase in the potential (voltage) upon discharging the cell. As a result, there is net energy production over the cycle extracted from the mixing process (Figure 1b).

Prior studies have primarily focused on understanding physics of the capacitive double layer extraction process, such as electrode properties [7-12], structure of the double layer [9, 13] , kinetics [14], temperature-based effects [15], and effects on electron valence [16]. However, investigation of the operation modes of the four-stage cycles has not been examined in detail. Experimental investigations have only investigated one cycle. The experimental CapMix cycle occurs using four processes. In process 1-2, electrodes are charged in the C_H solution (e.g. constant concentration). In process 2-3, a C_L solution replaces the C_H solution (constant charge). In process 3-4, the electrodes are discharged. Finally, in process 4-1, the C_L solution is replaced by the C_H (constant charge) [5, 15, 17-22]. Here we will theoretically examine the operations of CapMix for ion mixing using thermodynamic principles. While previous investigations have focused on exploring the thermodynamic limits associated with Carnot and Stirling based analog cycles [5], we aim to extend this to investigate Otto, Diesel, Brayton, Atkinson, and Ericsson analogs. Fundamentally, we will seek to explore the effect operational modes have on maximizing efficiency and work output from CapMix cycles.

For the goals of our study, we seek to address the following fundamental questions:

- 1. What is the effect of different operational modes (e.g. constant V vs. constant σ vs. constant N) on the performance (work output, efficiency) of CapMix cycles?
- What is the effect of different operating parameters (water recovery, charge/discharge voltage ratio) for

maximizing the efficiency and work output of CapMix processes?

METHODOLOGY

Most theoretical heat engine analyses evaluate energy production through cycles comprised of four processes. Often these processes take place while keeping system properties constant. For instance, processes take place under isothermal (iso-T), isentropic (iso-s), isochoric (iso-V), and isobaric (iso-P) conditions where T, s, V, and P refer to temperature, entropy, volume and pressure. When considering electrochemical properties, we evaluate four analogous properties: chemical potential μ , number of ions N, charge σ , and voltage -V_{cell} [6]. Consequently, here we will be interested in evaluating processes that take place under iso- μ , iso-N, iso- σ , and iso- V_{cell} conditions. Since the thermal analog for voltage is the negative of pressure, this indicates that a mixing cycle will operate in the counterclockwise direction when viewed on a $V_{\text{cell}}\!\!-\!\!\sigma$ diagram [5, 17, 23].

The chemical potential μ varies as a function of both concentration and temperature

$$\mu = k_B T ln \left(\frac{c}{c_{ref}}\right) \tag{1}$$

where k_B is Boltzmann's constant and C_{ref} is a reference temperature to the environment, here taken as 1 M [5]. Here, since all simulations take place under standard conditions (temperature and pressure), all constant chemical potential processes are also constant concentration processes.

The total number of ions in the cell (per electrode area), N,

$$N = \Gamma + CL_e N_{av} \tag{2}$$

where N_{av} is Avogadro's constant, L_e represents the pore length between carbon particles (pore volume/pore area), taken in this study as 4 nm, and Γ is the excess surface charge. Γ is determined as a function of both the electrode surface charge σ and additional crossover charge σ*

$$\Gamma = \sqrt{\sigma + \sigma^*} - \sigma^* \tag{3}$$

$$\Gamma = \sqrt{\sigma + \sigma^*} - \sigma^*$$

$$\sigma^* = \frac{1}{2\pi\lambda_B\lambda_D}$$
(3)

where the Debye and Bjerrum lengths for the electrolyte, λ_B and λ_D , determine the crossover charge $\sigma^*[21]$. Crossover charge is defined as the charge at which attractive forces from counter ions and repulsive forces from co-ions are balanced [24]. When crossover charge exceeds surface charge, the increase in counter ions exceeds the decrease in concentration of co-ions, resulting in a net increase in number of ions adsorbed [25]. As surface charge decreases, Γ becomes directly proportional to σ . The diffuse layer voltage difference ΔV_D is

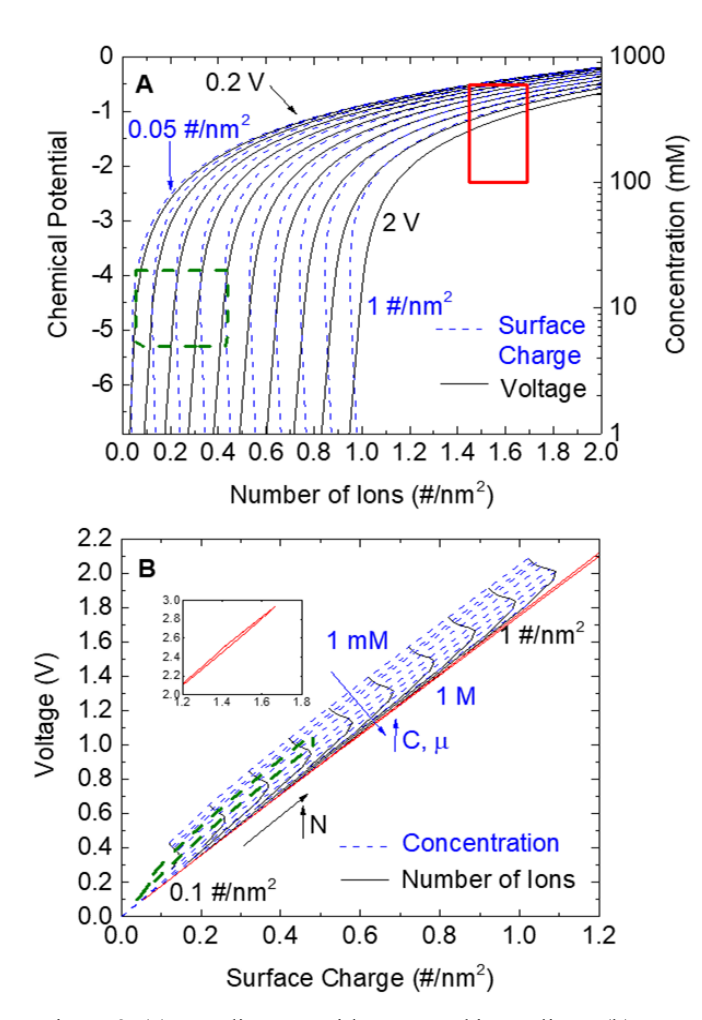


Figure 2. (a) μ -N diagram with Iso- μ and iso-N lines. (b) V_{cell} - σ diagram with iso-N and iso-C lines. Red solid and green dashed box designate Carnot cycle at high concentration (red solid) and low concentration (green dashed).

$$\Delta V_D = 2V_T \sinh^{-1} \left(\sigma \sqrt{\frac{\pi \lambda_B}{2CN_{av}}} \right) \tag{5}$$

with thermal voltage V_T defined as $V_T = RT/F$, where F is Faraday's constant. For the Stern layer voltage ΔV_{st} , Gauss' law is used for a 1:1 electrolyte (as in the case with NaCl):

$$\Delta V_{st} = \frac{\sigma e}{c_{st}} \tag{6}$$

where C_{st} is the Stern capacity and e is the elementary charge. For C_{st} , we will use values from previous studies with Gouy-Chapman-Stern models which have assumed a constant Stern capacity around 0.08 F/m^2 [26, 27]. Assuming a symmetric cell configuration, summing and doubling the Stern and diffuse layer potentials yields the total voltage through the cell ΔV_{cell}

$$V_{cell} = 2(\Delta V_{st} + \Delta V_D) \tag{7}$$

The interdependence of the four properties (μ , N σ , V_{cell}) to one another are most clearly displayed on a μ -N or V_{cell}- σ diagram which is analogous to a T-s and P-V based diagrams commonly used to evaluate thermal based processes (Figure 2a and b). T-s diagrams contain lines of constant pressure (isobars), and P-V diagram contains lines of constant temperature (isotherms). Here, we plot both lines of constant charge (iso- σ) and voltage (iso-V_{cell}) on the V_{cell}- σ diagram, and lines of constant concentration (iso-C) and number of ions (iso-N) on the μ -N diagram. The iso-V_{cell} and iso- σ lines are nearly identical (black and blue dashed lines), and at lower concentrations begin to align with an iso-N processes (vertical line) (Figure 2a).

At low concentrations (e.g. C<100 mM), the area of a Carnot cycle, which represents work output, does not change substantially. The Carnot cycle for blue energy systems employs two iso- μ (charge/discharge) processes (process 1-2 and 3-4), and two iso-N switching processes (process 2-3 and 4-1) (Figure 1). The μ is nondimensionalized by dividing it by room temperature (T = 298 K) and Boltzmann's constant (Figure 2). When the concentration is large (C>100 mM), N grows exponentially with respect to chemical potential. This allows for an increase in the area of the Carnot cycle, and highlights the benefits of operating a cycle under Carnot-like conditions.[20, 21, 23].

For CapMix, we will simulate various combinations of iso- μ , σ , V_{cell} ,N processes at a range of salinity gradients (e.g. ΔC) and aim to evaluate the efficiency by which chemical mixing energy is converted to electrical energy. The cycle efficiency is defined here as the first law (energy) efficiency η_E , η_E is defined as the net cycle work output $E_{net} = \oint V d\sigma$ to the input work E_{in} consumed during the charging stage only:

$$\eta_E = \frac{E_{net}}{E_{in}} \tag{8}$$

We verify the appropriate energy balance during the cycle by considering not only the electrical work gained or lost during each process, but also the change in free (chemical) energy, given as $\oint \mu dN$. Over the entire cycle, the integrals $\oint \mu dN$ and $\oint V d\sigma$ should sum to 0, indicating appropriate energy balance is reached [5]. To evaluate effectiveness of ions exchanged within the cell, we will compare the net output work E_{net} to the maximum range of the number of ions during the cycle:

$$W'_{N} = \frac{E_{net}}{\Delta N} \tag{9}$$

where ΔN represents the range between the maximum and minimum number of ions exchanged during the cycle. We will also evaluate the second law (thermodynamic) efficiency η_{th} for the CapMix process by comparing the net cycle work to the maximum obtainable energy from the mixing ΔG_{mix} :

$$\Delta G_{mix} = -2RT \left(\frac{c_M}{\phi} \ln(x_M) - C_L \ln(x_L) - \frac{1-\phi}{\phi} C_H \ln(x_H) \right)$$
 (10)

where φ is the volume fraction of low and high concentration mixed. The mole fractions $x_M,\,x_L,$ and x_H all correspond to the mole fraction of the exit mixture (M), and input low (L) and high (H) concentration solutions. We will always assume this value as $\varphi=0.5.$ We will also assume activity coefficients as unity. Thus, the second law efficiency η_{th} is given as:

$$\eta_{th} = \frac{E_{net}}{\Delta G_{mix}} \tag{11}$$

Stages with a constant number of ions are analogous to isentropic process in thermodynamics, or, in the case of reversible cycles, also analogous to adiabatic (no heat transfer) processes. To develop fully reversible cycles, we will run the cycles under infinitely slow conditions by linearly scaling a chosen parameter during each process from the initial state to the desired value at the next state (e.g. maximum voltage or minimum concentration). This is traditionally done for thermodynamic processes to eliminate irreversibilities due to transients [2].

We will develop analogies for seven thermodynamic cycles: Otto, Diesel, Brayton, Atkinson, Ericsson, Stirling, and Carnot. We provide the analog thermodynamic properties for each cycle (Table 1). In the CapMix process 1-2 the cycle is charged using a iso-µ (Ericsson, Stirling, Carnot cycles) or iso-N (Otto, Diesel, Brayton, Atkinson cycles) process, until V_{max} (V_{max}= 1 V). Next in Process 2-3, switching from C_H to C_L occurs at iso-V (Diesel, Brayton, Atkinson, Ericcson), iso-σ (Otto, Diesel, Stirling. Atkinson), or iso-N (Carnot). If voltage is not constant, the cell voltage can increase during Process 2-3. Hence, a cutoff voltage for process 2-3 was set as 1.0 V, below the threshold for water splitting (1.2 V) [28]. In process 3-4 the cycle is discharged through a iso-µ (Ericsson, Stirling, Carnot cycles) or a iso-N (Otto, Diesel, Brayton, Atkinson cycles) process until the minimum voltage V_{min} (V_{min}=0.1 V). The cell concentration will gradually increase during this discharging stage. Finally, in Process 4-1, switching from C_L back to C_H occurs at iso-V (Diesel, Brayton, Atkinson, Ericcson), iso-σ (Otto, Diesel, Stirling. Atkinson), or iso-N (Carnot). We will evaluate and compare the performance dependence of each of the cycles (Table 1) as a function of ranges in concentration ($\Delta C = C_H - C_L$) and voltage ($\Delta V = V_{max} - V_{min}$).

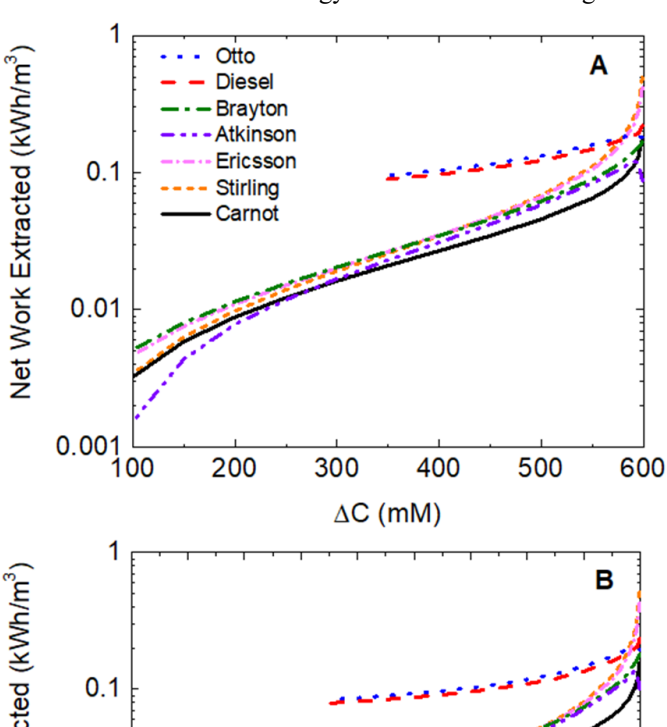
RESULTS AND DISCUSSION

For all CapMix cycles, increasing the ΔC resulted in a clear increase the net work (Figure 3a and b). With $C_H = 600$ mM the maximum extracted work ranged from an average 0.01 - 0.2kWh per m³ depending on the choice of $C_L = 1-500$ mM (Figure 3a), averaged over all of the different cycles. With $C_H = 1$ M the maximum extracted work increased slightly to 0.03 - 0.3 kWh per m³ for $C_L = 1-900$ mM (Figure 3b), again averaged per the

Table 1. Equivalent constant cycling conditions for thermodynamic and blue energy harvesting.

Cycle	Constant Terms (thermodynamic)	Constant Terms (electrochemical)
Otto	S, V	Ν, σ
Diesel	S, V (low T), P (high T)	N, σ (low μ), V_{cell} (high μ)
Brayton	S, P	N, V _{cell}
Atkinson	S, P (low T), V (high T)	N, V_{cell} (low μ), σ (high μ)
Ericcson	T, P	μ, V_{cell}
Stirling	T, V	μ, σ
Carnot	T, S	μ, Ν

type of cycle. This increase in extracted work is due to an increase in available energy released due to mixing (ΔG_{mix}). For instance the theoretical energy released from mixing C_H =600 mM with C_L =100mM (ΔC =500 mM) is 0.27 kWh per m³, whereas the theoretical energy released from mixing C_H =1M



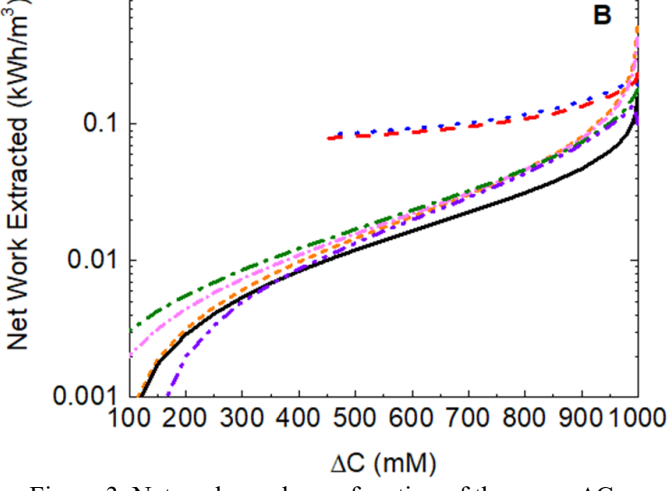


Figure 3. Net cycle work as a function of the range ΔC between the maximum concentration C_H and minimum concentration C_L (a) $C_H = 600$ mM, (b) $C_H = 1$ M.

with C_L =500 mM (ΔC =500 mM) is 0.1 kWh per m³ (Figure 3b).

As $\Delta C \rightarrow C_H$, iso- μ charge/discharge (Process 1-2 and 3-4) employed in the Ericsson, Stirling and Carnot cycles are more advantageous for work output than charge/discharge processes which take place under iso-N conditions (Otto, Diesel, Brayton, Atkinson). This is due to the large hysteresis (separation) between charge and discharge profiles attainable with the iso- μ process when compared to profiles projected with iso-N processes. Large hysteresis results in a larger area as projected on a V_{cell} - σ or μ -N diagrams (Figure 3a and b). With C_H = 600 mM and ΔC =599 mM, this maximum extracted work (e.g. area of cycle curve) is 0.49 kWh/m³ for the Stirling cycle. This was followed by 0.42 kWh/m³ for the Ericsson cycle, 0.18 kWh/m³ for the Carnot cycle and Otto cycle, 0.22 kWh/m³ Diesel, 0.17 kWh/m³ Brayton, and 0.08 kWh/m³ Atkinson cycles (Figure 3a). When a brine solution as considered for high concentration, a

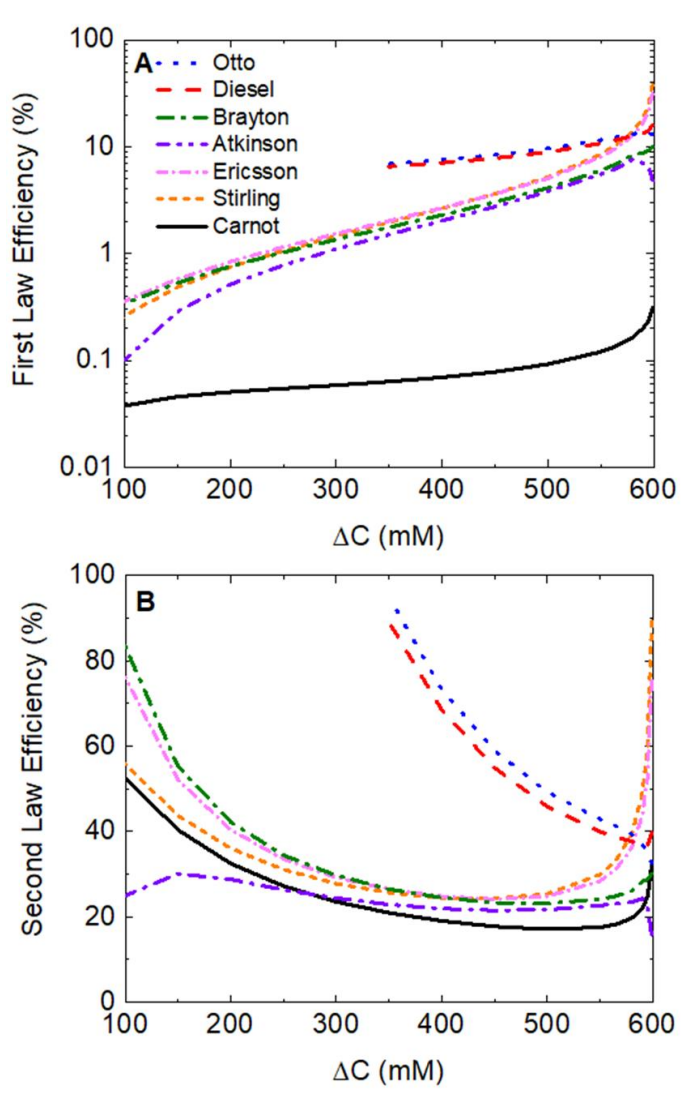


Figure 4. Effect of concentration range on efficiency with a seawater concentration ($C_H = 600 \text{ mM}$) as the maximum value. (a) first law efficiency, (b) second law efficiency.

slight increase in the work output is observed (Figure 3b). Net work outputs increased to (in kWh/m³): 0.51 (Stirling), 0.43 (Ericsson), 0.16 (Carnot), 0.19 (Otto), 0.18 (Brayton), 0.23 (Diesel), 0.10 (Atkinson).

The Carnot cycle did not result in the greatest net work output, first law, or second law efficiency. However, it did result in the greatest work per ion exchanged. The lower Carnot cycle performance is attributed to the trajectory of a iso-N process with respect to V_{cell} (Figure 3b). During an iso-N switching stage (process 2-3 and 4-1), the cell voltage continues to rise until the maximum voltage (a fixed boundary condition). Upon reaching the maximum voltage, in order to maintain the constant N, the charge must decrease (Eqn. 2). As a result, the charge in the cell is lower for the Carnot cycle at the beginning of the discharge process than it is for the Stirling cycle. This results in less energy recovery during Process 3-4. Additionally, after discharge, the iso-N line limits the minimum voltage that the cell can achieve before beginning the next switch stage. As a result, the work extracted during the discharge process reduces when compared to discharging to the constant voltage stage as is conducted in the Ericsson cycle. By comparison, as ΔC decreases, the difference in net work output between cycles reduces. At most, the cycles differ only by 20% for ΔC < 300 mM.

Evaluating the cycle efficiencies yields similar trends. For the C_H =600 mM, the first law (electrical) efficiency approached a maximum of 38% (Stirling), 31% (Ericsson), 16% (Diesel), 13% (Otto) 10% (Brayton), and 5% (Atkinson) (Figure 4a). The efficiencies decrease rapidly when ΔC <400 mM, which is due to the decreased thermodynamic work potential obtainable from mixing (ΔG_{mix}). Increasing C_H to 1 M, the maximum first law efficiencies obtained changed only slightly: 22% (Stirling), 17% (Ericsson), 8% (Otto), 6% (Brayton), 0.1% (Carnot), 9% (Diesel), 3% (Atkinson).

The Stirling cycle outperformed the Ericsson cycle, which we attribute to the fact that the constant charging stage does not

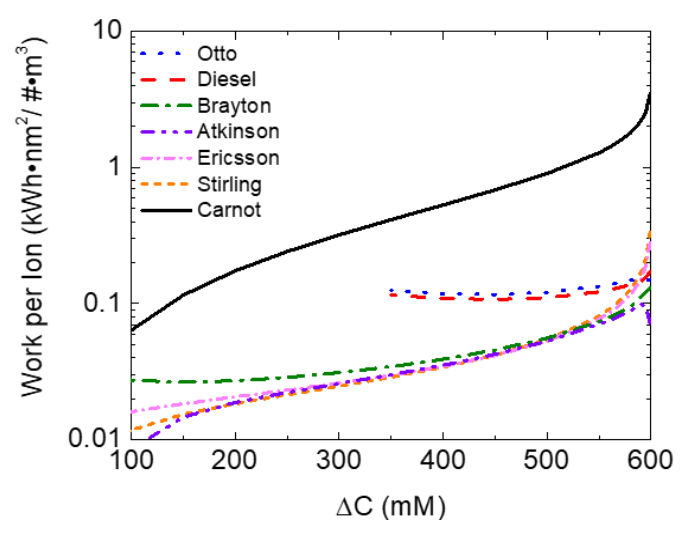


Figure 5. Net cycle work per number of ions exchanged as a function of ΔC ($C_H = 600$ mM).

require any additional input work, and the constant charge, switch process enables higher discharge voltage, improving the net work output. The Carnot cycle stands out as an anomaly again, exhibiting lower efficiency values of 0.3% (Figure 4a). This demonstrates one of the challenges in constant number of ions as a switching stage.

The Stirling and Ericsson cycles also exhibit maximum second law efficiency (percent of maximum available mixing energy converted to electrical energy). Both approach a maximum second law efficiency of 80% (C_H =600 mM and ΔC =599 mM), while the Carnot cycle approaches 50% (Figure 4b). Thus, each cycle operates irreversibly as all second law efficiencies remained below 100%. However, as ΔC $\rightarrow C_H$, the Stirling, Ericsson, and Carnot cycles appear to approach 100%, which would indicate a perfectly reversible system.

With the exception of the Atkinson and Brayton cycles, the second law efficiencies also demonstrate a second maximum when C_L approaches C_H ($\Delta C \rightarrow 0$). This depicts the exponential decline in the ΔG_{mix} , which reduces to zero as the $\Delta C \rightarrow 0$. In this limit despite the second law efficiency approaching 100%, the work output also decreases to a not useful level. Thus, it is theoretically possible through cycle operation to obtain over 50% of the theoretical energy from mixing, despite current technologies that only capture at best 50% of the ΔG_{mix} [29, 30].

For the Otto and Diesel cycles, there is a limit to the minimum ΔC by the Gouy-Chapman Stern theory; if operating under a constant number of ions, charging the cell to a certain voltage requires some removal of the initial salt concentration to maintain the iso-N condition. Thus, reducing the salt removal any further would not be possible, and would result in net work outputs larger than the Gibbs energy of mixing (Figure 4b).

The benefits of the Carnot cycle operation are more clearly pronounced when examining the ratio of work output per number of ions exchanged, W'/ ΔN , or effectiveness. When diluting to brackish concentrations ($C_H = 600$ mM, $C_L = 100$ mM, $\Delta C = 500$ mM), ΔN varies by 15% when iso- σ or iso- V_{cell} conditions are

employed. For most other cycles, this large range in number of ions greatly reduces the W'/ΔN. As a result, the W'/ΔN for all non-Carnot cycles only reaches 0.1 ± 0.05 kWh•nm²/#m³ for C_L= 20 mM and up to 0.2 ± 0.1 kWh•nm²/#m³ in the limit of low However, C_L . when employing σ charging/discharging with iso-N switching, the W'/ Δ N increases by approximately 10x (from 0.3 to 3.5 kWh•nm²/#m³⁾ for Carnot when compared to all other cycles (Figure 5). The second highest value of 0.3 kWh•nm²/#m³ for W'/ΔN was obtained by the Stirling cycle. This reaffirms one of the previously cited advantages of the Carnot-like mixing engine. Thus, while the Carnot cycle first law efficiency may have been low from an energy perspective, it displayed more benefits when considering the effective usage of ions within the cell, especially when operating at higher concentration ranges.

One notable feature is that in the Otto and Diesel cycles, the number of ions grows asymptotically as $\Delta C \rightarrow 0$. This is indicative of the limitations of the constant number of ions condition in Eq. (2). The maximum voltage set in the cycle inherently requires a minimum number of ions removed during the charging stage. If the amount removed in this charging stage is close to the desired minimum concentration C_L , then the switching stage is not necessary and the number of ions will subsequently change minimally. This is since the lines for constant charge and voltage are nearly parallel to the constant number of ions lines at low concentrations (Figure 2a). Such operations are of minimal interest, as they will not generate energy. Nevertheless, as with the minimum observed for second law efficiency, we make note of this additional unique trait during these cycle operations.

Lastly, we vary the input voltage ratio while maintaining all other appropriate cycle parameters. Since the cycle assumes an infinitely slow operation, C_H , C_L , and ΔC remain fixed at 600 mM, 20 mM and 580 mM. For mixing seawater with river water, the increase for net work extracted grows proportionally, employing a iso- μ charging/discharging over the range of ΔV simulated (0.1 V < ΔV < 1.1 V).

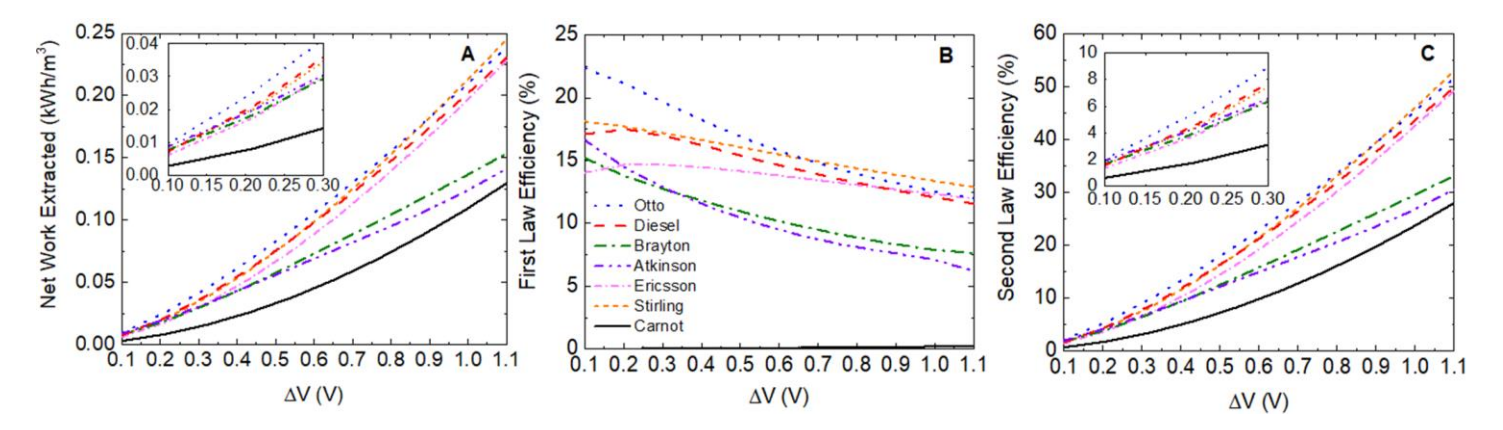


Figure 6. Net cycle work as a function of the voltage range ΔV . Effect of varying voltage range ΔV between minimum (initial) cycle voltage at Stage 1 and maximum cycle voltage at Stage 2. (a) Net cycle work, (b) first law efficiency, (c) second law efficiency. $C_H = 600$ mM, $C_L = 20$ mM.

For all ranges of ΔV the work output was higher for the Otto/Stirling> Diesel/Ericsson> Brayton/Atkinson> Carnot cycles (Figure 6a). This suggests that in addition to higher concentration ranges, the Carnot cycle should operate when considering higher voltage ranges to approach the work output of the other cycles. Additionally, at this concentration range selected a notable benefit in Otto/Diesel cycle operations showed in the lower voltage ranges.

When examining cycle efficiencies as a function of voltage, the lower voltage ranges predominantly demonstrate the highest first law efficiencies. Instead of continuously increasing to 100%, it seems that some of cycles actually demonstrate clear peak values. For example, the Stirling cycle approaches a maximum of 18% efficiency, but the Ericsson cycles only maximum at about 15% at a ΔV of around 0.3 V (Figure 6b). The Otto cycle more clearly highlights the benefits of constant charge switching when coupled with a constant number of ions. Its efficiency grows to a maximum of 23%, 5% higher under any other cycle with the same concentration and voltage ranges. Some of the other cycles lower maximum efficiencies of around 0.2 V before beginning to decrease in the limit of ΔV (17% for Diesel cycle, 16% for Atkinson cycle, 15% for Brayton cycle). The Carnot cycle, however, is the only one that increases when consuming more voltage during the charging stage. Despite this, all of the other cycle efficiencies remain at least 2x as large as the maximum Carnot cycle efficiency. Thus, it is possible that tailoring the cycle could enable operations at higher voltages and/or increases first law efficiency to a point where Carnot operation could surpass the other cycles.

Since concentration ranges remain the same when sweeping voltage range, the second law efficiency is exactly proportional to the net cycle work (Eq. 11). Compared to the previous cycles with V_{max} fixed at 1 V ($\Delta V = 0.9$ V), if the voltage range were expanded, it could reach maximum efficiency of over 50% when operating a mixing Stirling engine (Figure 6c). A caveat to operating here is that since we only account for cell voltage after the initial charging stage, the additional ~0.1-0.2 V incurred during constant charge switching would push V_{cell} above the operating threshold for electrolysis. While most studies for CapMix have typically operated under lower voltage ranges, this voltage rise needs to be considered if the operating range is to be expanded [17].

CONCLUSION

Simulating different operation for CapMix cycles suggested certain ways for optimizing performance. The cycles demonstrated a maximum efficiency and net work output when charging at constant chemical potential (concentration) and constant charging switching (Stirling engine). This maximized the overall recoverable energy (η_E = 38%, η_{th} = 89%) while eliminating additional input energy during switching (Net work output = 0.3 kWh/m³). Benchmark efficiencies for suitable brackish water ranges still yielded work output values from

 $0.03-0.2~kWh/m^3$ (20 mM < C_L < 200 mM). When raising the maximum concentration from a seawater value to a more concentrated solution, energy extracted on average could increase by up to 5%, although the Carnot cycle experienced a decrease.

While a Carnot-like operation with constant switching mode does not recover energy as effectively (maximum work output = 0.18 kWh/m³), its efficiency per number of ions exchanged during cycling is higher (3.3 kWh•nm²/#•m³, over 10x greater than maximum for all other cycles). The increase in work output per number of ions is attributed to the substantial change in the number of ions during an iso-σ or iso-V process. Through thermodynamic principles, we have defined an extensive range of operating conditions and parameters for EDL capacitors. The results obtained provide unique insight on the conditions that cycles should operate at depending on the desired system criteria (work output, first and second law efficiency). Developing thermodynamic analogies such as the ones presented in this study can improve our understanding and performance of a wide range of cyclic energy processes. Future studies will aim to investigate further into exergetic and economic analysis of the different cycling modes of operation.

ACKNOWLEDGEMENTS

This material is based upon work supported by the National Science Foundation under Grant No. (1821843) for MCH. This work is also supported by the ARCS graduate fellowship to Daniel Moreno.

REFERENCES

- [1] K. Hussey and J. Pittock, "The energy-water nexus: Managing the links between energy and water for a sustainable future," 2012.
- [2] M. J. Moran, H. N. Shapiro, D. D. Boettner, and M. B. Bailey, *Fundamentals of engineering thermodynamics*: John Wiley & Sons, 2010.
- [3] J. W. Post, Blue Energy: electricity production from salinity gradients by reverse electrodialysis, 2009.
- [4] G. R. Iglesias and M. M. Fernández, "Capacitive Energy Extraction From CDLE: Implementation," in *Interface Science and Technology*. vol. 24, ed: Elsevier, 2018, pp. 119-140.
- [5] N. Boon and R. Van Roij, "'Blue energy'from ion adsorption and electrode charging in sea and river water," *Molecular Physics*, vol. 109, pp. 1229-1241, 2011.
- [6] R. van Roij, "Statistical thermodynamics of supercapacitors and blue engines," *Electrostatics of Soft and Disordered Matter*, vol. 263, 2014.
- [7] X. Kong, A. Gallegos, D. Lu, Z. Liu, and J. Wu, "A molecular theory for optimal blue energy extraction by

- electrical double layer expansion," *Physical Chemistry Chemical Physics*, vol. 17, pp. 23970-23976, 2015.
- [8] C. Lian, X. Kong, H. Liu, and J. Wu, "On the hydrophilicity of electrodes for capacitive energy extraction," *Journal of Physics: Condensed Matter*, vol. 28, p. 464008, 2016.
- [9] K. Sharma, Y.-H. Kim, S. Yiacoumi, J. Gabitto, H. Z. Bilheux, L. J. Santodonato, et al., "Analysis and simulation of a blue energy cycle," *Renewable Energy*, vol. 91, pp. 249-260, 2016.
- [10] M. C. Hatzell, M. Raju, V. J. Watson, A. G. Stack, A. C. Van Duin, and B. E. Logan, "Effect of strong acid functional groups on electrode rise potential in capacitive mixing by double layer expansion," Environmental science & technology, vol. 48, pp. 14041-14048, 2014.
- [11] M. C. Hatzell, K. B. Hatzell, and B. E. Logan, "Using flow electrodes in multiple reactors in series for continuous energy generation from capacitive mixing," *Environmental Science & Technology Letters*, vol. 1, pp. 474-478, 2014.
- [12] D. Moreno and M. C. Hatzell, "Influence of Feed-Electrode Concentration Differences in Flow-Electrode Systems for Capacitive Deionization," *Industrial & Engineering Chemistry Research*, vol. 57, pp. 8802-8809, 2018.
- [13] D. Moreno and M. C. Hatzell, "Efficiency of Carnot and Conventional Capacitive Deionization Cycles," *The Journal of Physical Chemistry C*, vol. 122, pp. 22480-22486, 2018.
- [14] M. Rossi, T. Wallmersperger, S. Neukamm, and K. Padberg-Gehle, "Modeling and simulation of electrochemical cells under applied voltage," *Electrochimica Acta*, vol. 258, pp. 241-254, 2017.
- [15] M. Janssen, A. Härtel, and R. Van Roij, "Boosting capacitive blue-energy and desalination devices with waste heat," *Physical review letters*, vol. 113, p. 268501, 2014.
- [16] D. Moreno, Y. Bootwala, W.-Y. Tsai, Q. Gao, F. Shen, N. Balke, *et al.*, "In Situ Electrochemical Dilatometry of Phosphate Anion Electrosorption," *Environmental Science & Technology Letters*, vol. 5, pp. 745-749, 2018.
- [17] D. Brogioli, "Extracting renewable energy from a salinity difference using a capacitor," *Physical review letters*, vol. 103, p. 058501, 2009.
- [18] M. A. Anderson, A. L. Cudero, and J. Palma, "Capacitive deionization as an electrochemical means of saving energy and delivering clean water. Comparison to present desalination practices: Will it compete?," *Electrochimica Acta*, vol. 55, pp. 3845-3856, 2010.
- [19] P. Biesheuvel and A. Van der Wal, "Membrane capacitive deionization," *Journal of Membrane Science*, vol. 346, pp. 256-262, 2010.

- [20] J. Zhang, K. B. Hatzell, and M. C. Hatzell, "A combined heat-and power-driven membrane capacitive deionization system," *Environmental Science & Technology Letters*, vol. 4, pp. 470-474, 2017.
- [21] P. Biesheuvel, "Thermodynamic cycle analysis for capacitive deionization," *Journal of colloid and interface science*, vol. 332, pp. 258-264, 2009.
- [22] P. Biesheuvel, B. Van Limpt, and A. Van der Wal, "Dynamic adsorption/desorption process model for capacitive deionization," *The journal of physical chemistry C*, vol. 113, pp. 5636-5640, 2009.
- [23] A. Härtel, M. Janssen, D. Weingarth, V. Presser, and R. van Roij, "Heat-to-current conversion of low-grade heat from a thermocapacitive cycle by supercapacitors," *Energy & Environmental Science*, vol. 8, pp. 2396-2401, 2015.
- [24] T. Markovich, D. Andelman, and R. Podgornik, "Charged Membranes: Poisson-Boltzmann theory, DLVO paradigm and beyond," *arXiv preprint arXiv:1603.09451*, 2016.
- [25] R. A. Rica, R. Ziano, D. Salerno, F. Mantegazza, R. van Roij, and D. Brogioli, "Capacitive mixing for harvesting the free energy of solutions at different concentrations," *Entropy*, vol. 15, pp. 1388-1407, 2013.
- [26] M. Marino, L. Misuri, M. L. Jiménez, S. Ahualli, O. Kozynchenko, S. Tennison, et al., "Modification of the surface of activated carbon electrodes for capacitive mixing energy extraction from salinity differences," *Journal of colloid and interface science*, vol. 436, pp. 146-153, 2014.
- [27] M. Simoncelli, N. Ganfoud, A. Sene, M. Haefele, B. Daffos, P.-L. Taberna, *et al.*, "Blue Energy and Desalination with Nanoporous Carbon Electrodes: Capacitance from Molecular Simulations to Continuous Models," *Physical Review X*, vol. 8, p. 021024, 2018.
- [28] W. G. Pell, B. E. Conway, W. A. Adams, and J. De Oliveira, "Electrochemical efficiency in multiple discharge/recharge cycling of supercapacitors in hybrid EV applications," *Journal of power sources*, vol. 80, pp. 134-141, 1999.
- [29] A. P. Straub, A. Deshmukh, and M. Elimelech, "Pressure-retarded osmosis for power generation from salinity gradients: is it viable?," *Energy & Environmental Science*, vol. 9, pp. 31-48, 2016.
- [30] F. Liu, T. F. Donkers, R. M. Wagterveld, O. Schaetzle, M. Saakes, C. J. Buisman, *et al.*, "Parallel up-scaling of Capacitive Mixing (CapMix) system enhances the specific performance," *Electrochimica Acta*, vol. 187, pp. 104-112, 2016.